CEBAF Program Advisory Committee Nine Proposal Cover Sheet

This proposal must be received by close of business on Thursday, December 1, 1994 at:

CEBAF
User Liaison Office, Mail Stop 12 B
12000 Jefferson Avenue
Newport News, VA 23606

Proposal Title

Nucleon Structure Study by Virtual Compton Scattering at High Momentum Transfer

Contact Person

Name: Vincent Breton
Institution: Laboratoire de Physique Corpusculaire
Address: Université Blaise Pascal de Clermont-Ferrand
Address:
City, State ZIP/Country: F-63177 AUBIERE CEDEX FRANCE
Phone: (011-33) 73-40-72-66 FAX: (011-33) 73-26-45-98
E-Mail → Internet: Breton@frcpn11.in2p3.fr

Experimental Hall: A Days Requested for Approval: 28

Hall B proposals only, list any experiments and days for concurrent running:

CEBAF Use Only

Receipt Date: 12/15/94 PR 94-106

By: gp

Nucleon structure study by Virtual Compton Scattering at high momentum transfer

J. Berthot, P.Y. Bertin, V. Breton, H. Fonvieille, G. Quemener, O. Ravel, Y. Roblin
LPC: Univ. Blaise Pascal/IN2P3 Aubiere, France
P. Chen, R. Ent, J. Gomez, J. LeRose, R. Michaels, S. Nanda, E.J. Offermann, A. Saha, B. Wojtsckhowski
CEBAF, Newport News, VA23606, USA
L. Elouadhriri
Christopher Newport University, Newport News, VA23606, USA
G. Audit, M. Bernheim, E. Burtin, G. Fournier, T. Gousset, P.A.M. Guichon, M. Guidal, N. D'Hose, S. Kerhouas, C. Marchand, J. Marroncle, J. Martino, J. Mougey, L. Murphy, P. Vernin
DAPNIA/SPhN CE Saclay, France
J. Van de Wiele
IPN Orsay, France
A. Afanasev
Kharkov Institute of Physics and Technology, Ukraine and CEBAF
D. Ryckbosch, R. Van de Vyver, L. Van Hoorebeke
Nucl. Phys.Lab., B9000 Gent, Belgium
C.E. Hyde-Wright, L.B. Weinstein, P. Ulmer.
Old Dominion University, Norfolk VA, 23529-0116, USA
Z.E. Meziani
Temple Univ., Philadelphia, PA 19122, USA
A. Nathan
Univ. of Illinois 61801 Urbana IL USA
J.M. Finn
College of William & Mary, Williamsburg, VA, USA
A. Gasparian
Yerevan Physics Institute, Yerevan, Armenia

Spokespersons: V Breton(contact) , C.E. Hyde-Wright.

Abstract

We propose to use the 6 GeV beam at CEBAF to make the first measurement of Virtual Compton Scattering above the resonance region. Virtual Compton scattering is a purely electromagnetic process calculable within different approaches of non perturbative QCD. The proposed measurements can be compared to the predictions of QCD sum rules, diquark models and even the Hard Scattering Picture of perturbative QCD. It also has the unique interest of allowing the measurement of the phase of the Compton diagram through the interference with the Bethe-Heitler diagrams.

1 Introduction

Determining the short distance structure of the proton is an important topic in our quest for an understanding of the strong interactions in terms of the fundamental quark and gluon degrees of freedom. Elastic virtual compton scattering ($e + p \rightarrow e+p+\gamma$) at high energy and moderately high momentum transfer is a powerful probe of nucleon structure. It is the natural complement to form factors, real compton scattering, and deep inelastic scattering.

The first proposal on Virtual Compton Scattering at CEBAF (PR 93-050) was submitted to PAC6 in June 1993. The parts of this proposal on Virtual Compton scattering below pion threshold and in the resonance region were approved by PAC7 in December 1993. For the part dedicated to exploratory measurements of Virtual Compton Scattering at high momentum transfer beyond the resonance region, PAC6 recommended resubmission later to take advantage of the upgrade of the CEBAF beam energy to 6 GeV.

We propose to use the CW 6 GeV beam at CEBAF to make the first measurements of virtual compton scattering (VCS) above the resonance region. We will use the two HRS spectrometers in hall A to detect the scattered electron in coincidence with the recoil proton. From the measured momenta k' and p' of the electron and proton, we reconstruct the four momentum q'_μ of the missing particle. VCS events are characterized by $q'^2_\mu = 0$. The VCS events are separated from *e.g.* coherent pion production events with $q'^2_\mu = m^2_\pi$.

In addition to the new experimental tools that CEBAF provides, we have new theoretical tools with which to study the VCS reaction. Perturbative QCD and QCD sum-rule calculations make predictions for the high energy VCS amplitude. In addition, the diquark model provides a bridge between pQCD and the constituent quark model. It appears to be a more successful model than the pure quark picture at present medium energies. In the CEBAF accessible energy domain, it is one of the hadronic scenarios we will be able to accurately test with VCS.

2 Physics Motivation

The experiment will measure the cross section for exclusive electroproduction of a real photon. To lowest order in the fine structure constant $\alpha \sim 1/137$, the process is described by the coherent sum of the amplitudes shown in Fig. 1. In the following γ^* or γ^v will denote the virtual photon of the VCS process. Note that the virtual photon of the Bethe-Heitler (BH) process has different kinematics than in the VCS case, although all final state particles have the same kinematics in the two processes. We denote by $\theta^{\gamma^*\gamma}$ the laboratory angle between γ^* and real photon (angle between

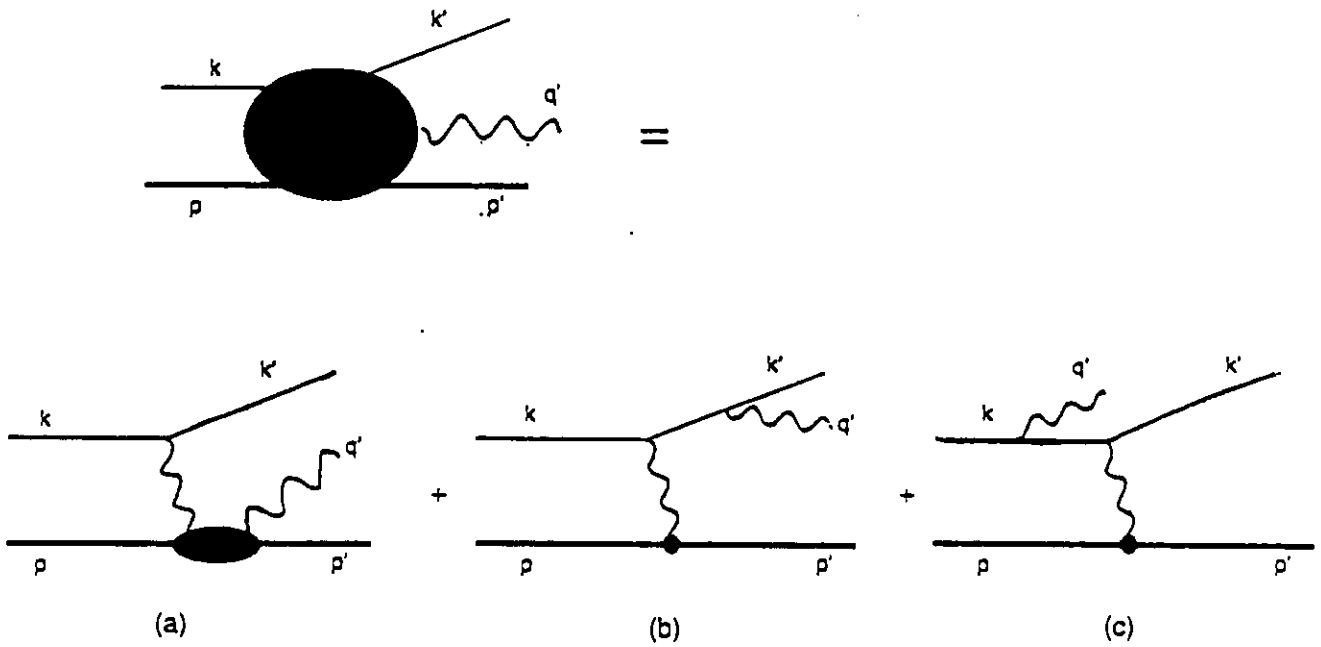

Figure 1: Feynman diagrams for the reaction $e + p \rightarrow e + p + \gamma$. The electron and proton momenta are k, k', and p, p', respectively. The final photon momentum is q'. a) Virtual compton scattering (VCS) amplitude. The virtual photon momentum is $q = k - k'$. We use the conventions $p^2 = p'^2 = M^2$, $Q^2 = -q^2$, $s = (p + q)^2$, $t = (q - q')^2 < 0$. The lab angle between q and q' is $\theta^{\gamma\gamma}$. b) & c), Bethe-Heitler (BH) terms with post- and pre- radiation, respectively. The virtual photon momentum is $q - q' = k - k' - q'$.

q and q'). We denote by θ_{CM} the same angle in the photon-proton center of mass frame. The transverse momentum of the real photon with respect to the virtual photon axis is simply :

$$P_t = \frac{s - M^2}{2\sqrt{s}} \sin\theta_{CM} \tag{1}$$

where M is the proton mass and t is the momentum transfer between the virtual and the real photon $(q - q')^2$. Our convention is that the azimuthal angle of the photon q' around the virtual photon q is $\phi = 0$ when q' is in the electron scattering plane on the same side of q as the scattered electron.

In Fig. 1, VCS refers to amplitude a) while b) and c) describe the BH process. The BH process is just the wide-angle radiative tail of elastic electron scattering. Hence the BH process is calculable once the elastic form factors $G_{Mp}(-t)$ and $G_{Ep}(-t)$ are known. This is the case in the energy range proposed here. As is well known, the BH process is strongly peaked along the electron lines. This allows us to define regions for the final photon (or recoil proton) where BH is either dominant, negligible, or of the same order of magnitude as VCS.

Since the BH amplitude is calculable, its interference with VCS is a new source of information, not present in either real compton scattering or in electroproduction experiments (e.g. $(e, e'p)\pi^0$).

In the rest of this section, we discuss only the VCS amplitude T_{VCS}. This amplitude depends upon three independent invariants. The usual choices are

$$Q^2,\ \ s,\ \ t \tag{2}$$

$$\text{or } Q^2,\ \ s,\ \ \theta_{CM} \tag{3}$$

2.1 Perturbative QCD and QCD sum rules

The perturbative approach to hard exclusive reactions may be motivated by a simple physical picture. Before the kick of the incoming e^- the proton constituents are sitting, in the proton rest frame, with low internal momenta (*ie* components of order a few hundred MeV[1]). This system has to absorb the virtual photon and soon emit the outgoing one, while the high momentum transfer is being shared coherently among all the constituents in the final state. This sharing out is mediated by (perturbative) exchange of at least one hard gluon between each pair of constituents.

Each hard gluon exchange introduces a factor of $1/t$ into the amplitude, where t is the invariant momentum transfer. We expect that to order M^2/t (equivalently

[1]in order to simplify our notations, we will use M, the proton mass, to designate typical mass scale in the problem.

M^2/s) the amplitude will be dominated by the simplest possible diagrams *i.e.* diagrams with the minimum number of soft constituents in the initial and final states (simplest Fock space configurations) and the minimum number of gluon exchanges, consistent with at least one hard gluon interaction with each soft constituent (the three quarks u, u, and d in the case of the valence Fock state of the proton).

These arguments lead naturally to the dimensional counting scaling law: in any exclusive reaction at sufficiently high energy at a fixed center-of-mass angle, the cross section scales as : [1]

$$\frac{d\sigma}{dt} = s^{2-n} f_x(\cos\theta_{CM}) \qquad\qquad s \gg M^2. \tag{4}$$

where s is the total invariant mass squared and n is the minimum number of external fundamental fields in the invariant amplitude. For elastic compton scattering on the proton, $n = 8$ (three quarks and a photon in the initial and final states). For the $p(\gamma, p)\pi^0$ cross section $n = 9$, thus the π^0 cross section should decrease more rapidly with s than the Compton cross section.

Fig. 2 displays a selected sample of high energy real compton data on the proton, for $t > 1GeV^2$. Although there are many experiments at high energy and low t, there is only the experiment of Shupe *et al.*, at large t [2]. The data are plotted as $s^6 d\sigma/dt$ *vs.* $\cos\theta_{CM}$ to illustrate the approach to the asymptotic scaling law. The most stringent test of the scaling law is obtained at $\theta_{CM} = 90°$. Fitting the data to a $s^{-\alpha}$ power law results in $\alpha = 7.0 \pm 0.4$: a 2.5σ deviation from the $\alpha = 6.0$ prediction.

There is more to pQCD than the scaling laws. There exist "parameter-free" calculations of high energy real[3, 4] and virtual compton scattering[5, 6] on the proton. In those works, the amplitude of the VCS is written as the convolution of three factors: the amplitude of a proton to exhibit its quark-gluon content (the incoming "wave function" which is first approximated by neglecting terms $O(M^2/|t|)$ and therefore restricting the study to the proton valence Fock state), the amplitude of the elementary process: $uud\gamma^* \rightarrow uud\gamma$ (the hard amplitude), and finally the amplitude of the 3 emerging quarks to reform a proton (outgoing wave function)

$$A = \psi_{(uud)} \otimes T_H \otimes \psi_{(uud)}{}', \tag{5}$$

where the convolution stands for a sum over discrete quantum numbers (color, flavor, helicities) and kinematically allowed quark momentum configurations. In this formula long-distance nonperturbative physics is isolated in the incoming and outgoing wave function. Wave functions are independent of the hard exclusive processes under focus and are the object one wants to address to understand how QCD builds up hadrons from quarks and gluons. These are separated from the short distance

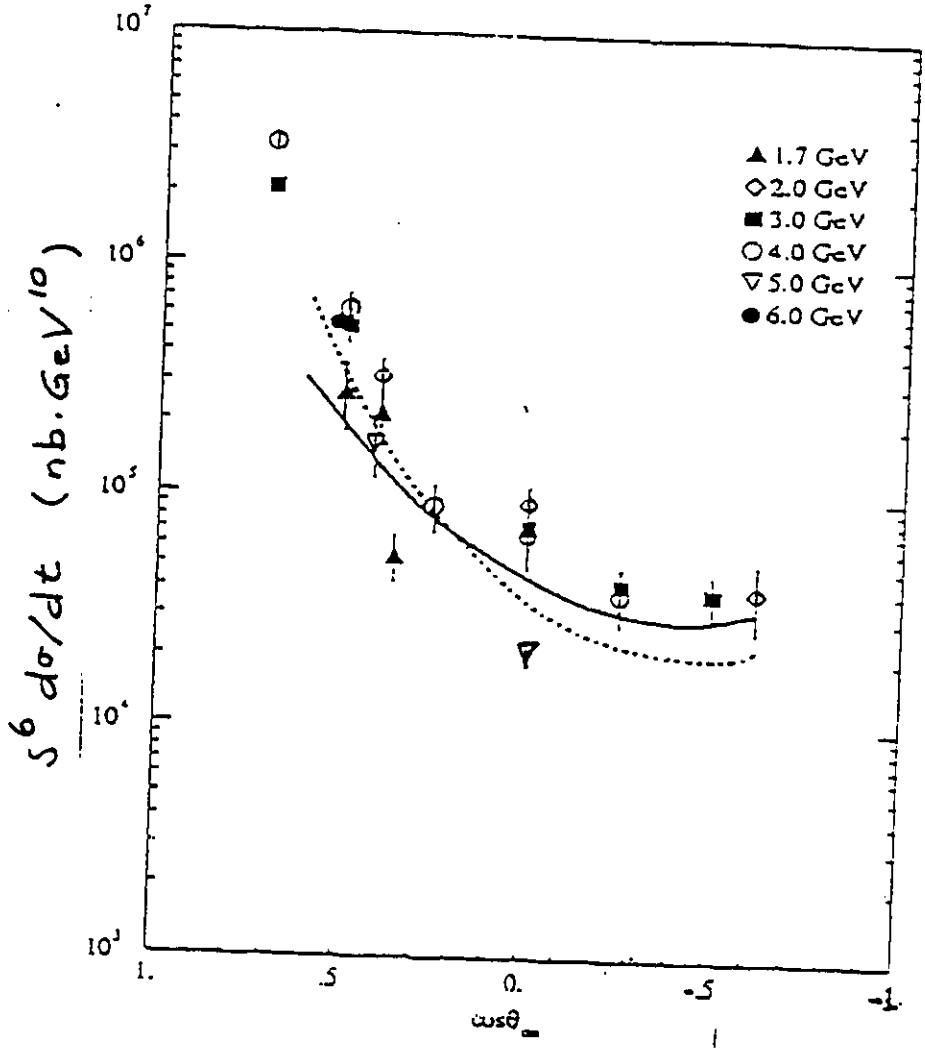

Figure 2: Selected sample of real compton $p(\gamma,p)\gamma$ data for $-t \geq 1.0$ GeV^2 [2]. The 2 curves are calculations within the diquark model for a laboratory energy of 4 GeV (solid) and 10.2 GeV (dotted).

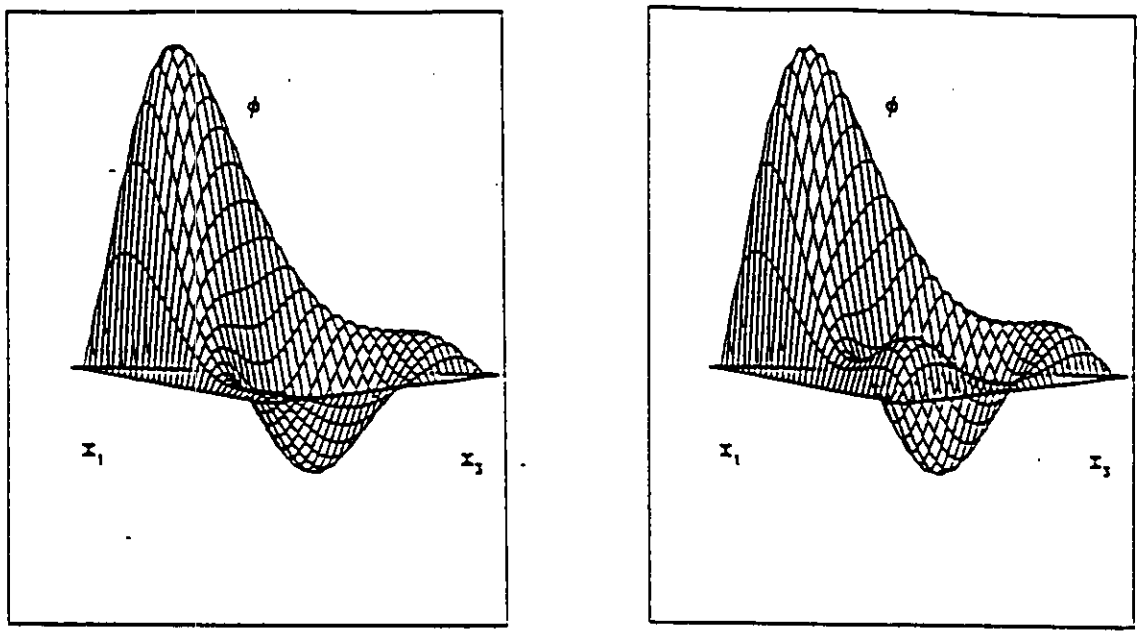

CZ

COZ

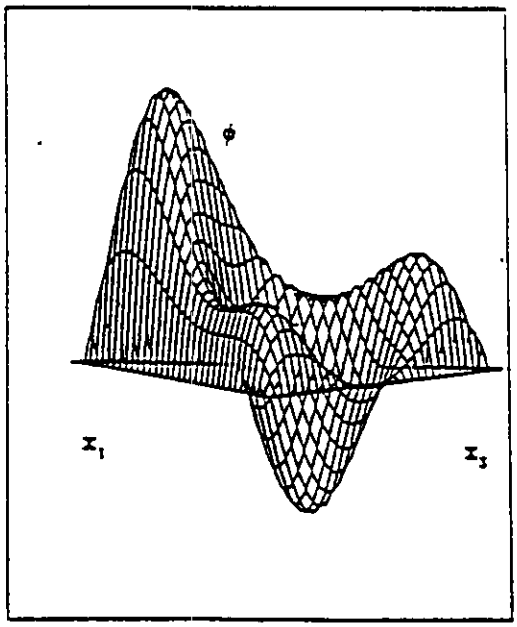

KS

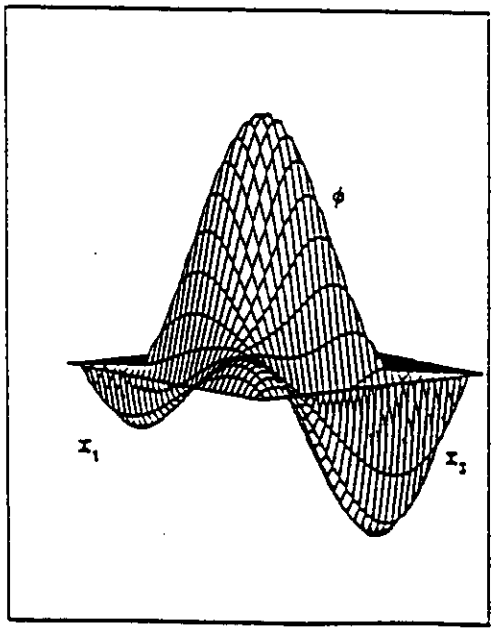

GS

Figure 3: The non-asymptotic distribution function of the proton, references contained in [4]. The labels refer to the authors C: Chernyak, O:Oglobin, Z: Zhitnitsky, K: King, S: Sachrajda, G: Gari, S: Stefanis.

subprocess amplitude described by T_H which may be computed within QCD perturbation theory. In this spirit, the above calculations keep only the lowest order Feynman diagrams (there are 336 non-vanishing topologically distinct ways to couple two photons to three quarks with the exchange of two gluons and 42 diagrams with the three gluon vertex whose color factor is, however, 0). Approximations done are: neglect of endpoint contributions (see later), and neglect of quark transverse momentum $\mathbf{k}_T$ in T_H, leading to a $\mathbf{k}_T$ integrated distribution amplitude

$$\phi(x_1, x_2, x_3) = \int [d\mathbf{k}_T] \psi(\{x_i\}, \{\mathbf{k}_{Ti}\}) \tag{6}$$

with the momentum conservation constraint

$$x_1 + x_2 + x_3 = 1. \tag{7}$$

By convention, $\phi(x_1, x_2, x_3)$ is the amplitude for the Fock space configuration $|u_+(x_1)u_-(x_2)d_+(x_3)\rangle$ with the $\pm$ subscripts identifying the quark helicity parallel or anti-parallel to the proton helicity. The amplitudes for the other spin-flavor configurations with the same momentum fractions are obtained from symmetry relations [4]. At sufficiently high momentum transfer, the distribution amplitude has the asymptotic form:

$$\phi_\infty(\{x_i\}) = 120 f_p x_1 x_2 x_3 \delta(1 - x_1 - x_2 - x_3) \tag{8}$$

where f_p is the wave function at the origin, the analogue of the pion decay constant f_π, and measures the capability of a proton to exhibit its three-valence-quark content. However, "The asymptotic distribution function ... is as apt at present energies as the asymptotic δ-function structure function "[4]. At finite s, $\phi(\{x_i\})$ is expanded in terms of ϕ_∞ times a polynomial in x_1, x_2, x_3. The polynomials are evaluated in the techniques of QCD sum rules, discussed below. The distributions from four commonly used distinct versions of the monomial expansion of ϕ are plotted in Fig. 3. In each case the distribution favors an up-quark with helicity parallel to the proton helicity carrying the dominant momentum fraction.

The pQCD calculations by Kronfeld and Nižić of real compton scattering are shown in Fig. 4. The large variations in ϕ lead to large variations in the compton cross section. In any case, the pQCD cross section with the asymmetric distribution amplitudes are an order of magnitude greater than with the asymptotic distribution amplitude (Eq. 8).

The distribution amplitudes of Fig. 3 are calculated by the techniques of QCD sum rules. In this approach, the soft physics is calculated by dispersion relations which connect the momentum space structure of the proton to a series of dispersion integrals over the excitation spectrum of the proton. The low-energy part of

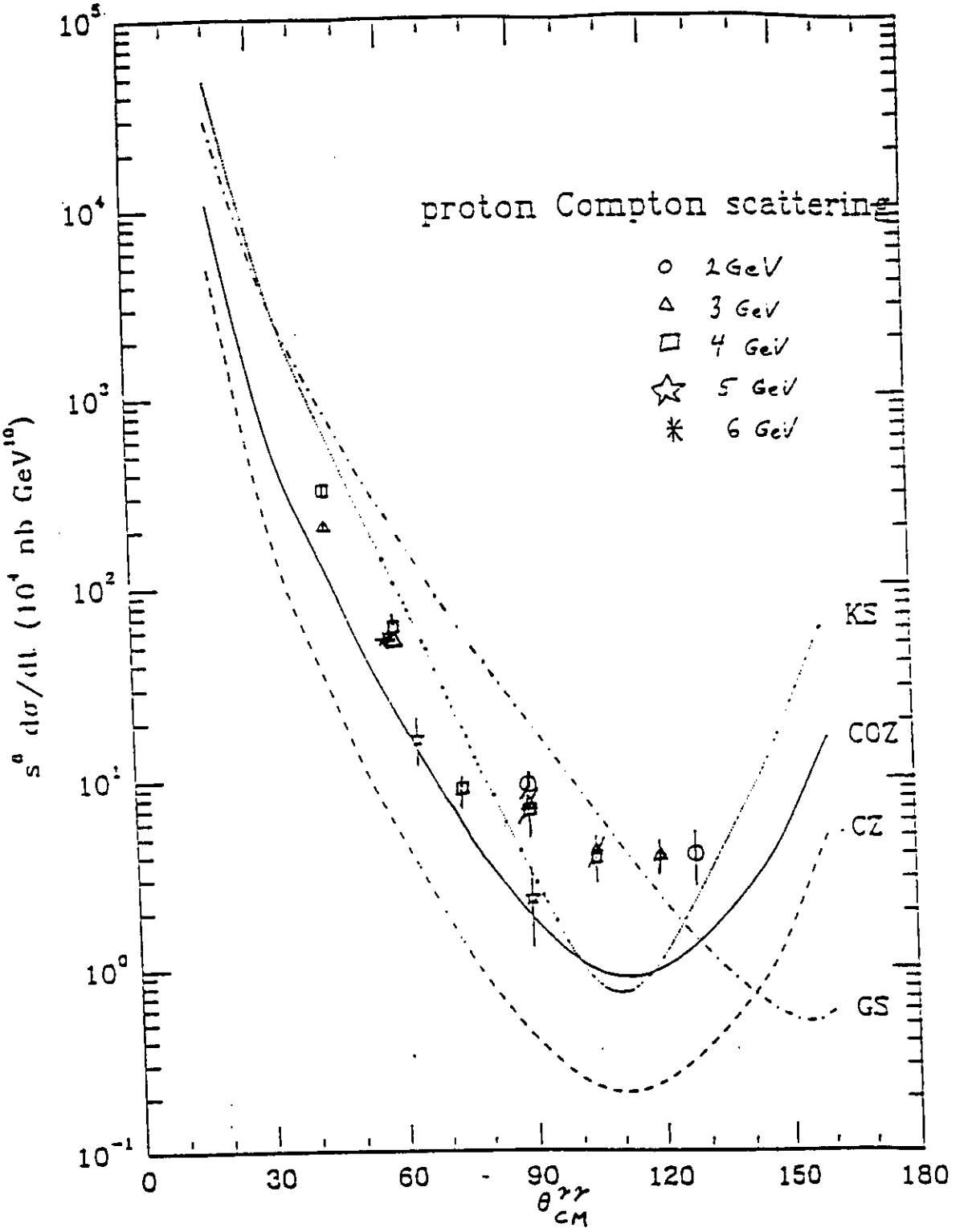

Figure 4: Real Compton data of [2] and pQCD calculations of [4], using the non-asymptotic distribution functions of Fig. 3.

the spectrum is treated phenomenologically and the high-energy part is treated in perturbative QCD.

The highly asymmetric distributions of Fig. 3 lead to large contributions to the pQCD calculations from regions of small x_i, or gluons with momentum-squared significantly less than $-t$. This has inspired new efforts to apply QCD sum rules directly to the compton process. In this way, the soft parts of the reaction process are treated on an equal footing with the wave function. Recently, the QCD sum rules were used to estimate the soft contribution in case of the real compton scattering on the pion [14]. Similar studies of the real and virtual compton scattering on the proton are now in progress [15].

2.2 Di-Quark Model

The diquark model of Kroll, Schürmann and Schweiger[7] follows the same basic procedure as the pQCD calculations outlined above. However, The constituents of the proton are taken to be a quark and a di-quark, rather than three quarks.

The diquarks are treated as quasi-elementary constituents which survive medium hard kicks. Their composite nature is taken into account by diquark form factors. Both scalar and vector di-quark configurations are included. Diquarks are an effective description of correlations in the wave functions and constitute a particular model for non-perturbative effects. The diquark model has been applied to a variety of processes and quite successfully confronted to data. Among these applications is a recent study of the electromagnetic nucleon form factors [7]. The diquark model is designed such that it gives asymptotically the scaling laws deduced from the quark picture.

We are going to shortly review its formulation and the interesting constraints provided by VCS on such a model [2].

For reasons already mentioned in the quark picture, a helicity amplitude for the process is an integral over momentum fraction

$$A = \phi \otimes T_H \otimes \phi', \tag{9}$$

where ϕ and ϕ' are respectively the incoming and outgoing proton distribution. More precisely the proton state, in the di-quark model, is a superposition of a q-S (S for Scalar diquark) and q-V (Vector diquark) state. The relative weight of these two states has been adjusted with the help of the magnetic proton form factor. Each state is fully described in term of its internal quantum numbers (spin, isospin, color), and

[2]Because of the relation between the diquark model and the pure quark picture, some of the following considerations may also apply to the last, even though accessible transfers seem to be too low to reliably compare VCS results with predictions from this framework.

the long range dynamics is parametrized with one S distribution amplitude, $\phi_S(x)$, and one V distribution amplitude, $\phi_V(x)$. These are functions of quark momentum fraction only, because the diquark fraction is fixed $(1-x)$ once the quark fraction is given. As a guidance one can integrate over x_2 in Eq. (8) to get an asymptotic form

$$\phi_{D\infty}(x) = 20 f_D x(1-x)^3, \tag{10}$$

$D = S$ or V; f_D has the same interpretation as f_p in the pure quark picture (see discussion after Eq. 8). The distributions proposed in [7] are slightly different from the above form, they are parametrized by a few quantities also adjusted to reproduce the magnetic form factor.

One of the interests of our experiment is the observation of the interference of VCS with the BH amplitude. This means that experimental data test the models at the amplitude level rather than at the cross-section level. In the diquark model, a non trivial phase structure occurs. It comes from the internal gluon propagator in graphs where the 2 photons attach to different legs (one on the quark, one on the diquark). The gluon momentum is then $k = \alpha p - \beta p' - q'$ with $\alpha = x$ or $1-x$ and $\beta = y$ or $1-y$. Thus, one gets for the gluon propagator

$$\frac{1}{k^2 + i\varepsilon} = \frac{1}{s\beta + \alpha(\beta t + u)} \tag{11}$$

which develops real and imaginary parts through the usual identity:

$$\frac{1}{k^2 + i\varepsilon} = PP(\frac{1}{k^2}) - i\pi\delta(k^2) \tag{12}$$

The imaginary part comes from the δ-function which specifies particular values of momentum fractions x or y and is thus very sensitive to the short and long range dynamics of the model.

The results of the diquark model for real compton scattering data from [2] are presented on figure 2. Although one may be surprised that, at so low energies, a model based on perturbative QCD still applies, the diquark model is seen to agree very well with data.

2.3 Physics program

We propose to start at CEBAF the study of the nucleon structure by Virtual Compton scattering at high momentum transfer. The extension of CEBAF beam energy up to 6 GeV opens up a phase space beyond the resonance region $s \geq 4(GeV/c)^2$ where several non perturbative QCD models make predictions. Since 1994, complete calculations of VCS amplitude and interference with Bethe-Heitler are available within the diquark model approach, and QCD Sum Rules calculations are under

way. The proposal intends at making the first measurements of Virtual Compton scattering amplitude and interference with Bethe-Heitler and therefore bring new stringent constraints on present non perturbative QCD models.

3 Experimental aspects

3.1 Method

As in the previous proposal [16], we propose to investigate VCS at high momentum transfer at CEBAF by detecting the scattered electron and proton in coincidence in the HRS spectrometers of Hall A. From the measured 4-momenta P_e and P_p and the incident beam energy E_i, we reconstruct the missing mass M_X :

$$M_X^2 = E_X^2 - P_X^2 \tag{13}$$

where,

$$E_X = E_i - E_e - E_p \tag{14}$$

$$\vec{P}_X = \vec{P}_i - \vec{P}_e - \vec{P}_p \tag{15}$$

The VCS events are characterized by the photon mass $M_X = 0$. The good resolution of HRS spectrometers allows a clean separation of VCS and π^0 events, and no detection of the photon is needed. Figure 5 shows the separation between the photon and the π^0 peak from our simulation of Hall A spectrometers.

In this proposal, we will use the two spectrometers of the hall A in their standard configuration as described in the table 4.1 of [10]. Standard electron and proton identification will be used. Thanks to the CEBAF high duty cycle, we are not limited by accidental $(e,e') \times (e,p)$ coincidence rates, nor by singles rates (0.5 MHz) and we will use therefore a luminosity of $2.10^{38}\ cm^{-2}s^{-1}$. This corresponds to $80\mu A$ beam current on a 10 cm long liquid hydrogen target. We will use the high power cryogenic target developed for the hall A. Its specifications can be found in table 8.3 of ref [10]. No modification of the vacuum target chamber is required.

3.2 Counting rates evaluation

The evaluation of Virtual Compton scattering cross section was done using a simple model deduced from real Compton data and a complete calculation within the diquark model. All the figures in this chapter showing results in the framework of the diquark model correspond to coplanar kinematics at $\phi = 0$.

Counting rates were obtained from the cross sections using a Monte-Carlo simulation of hall A spectrometers [12] and a luminosity of $2.10^{38}\ cm^{-2}s^{-1}$.

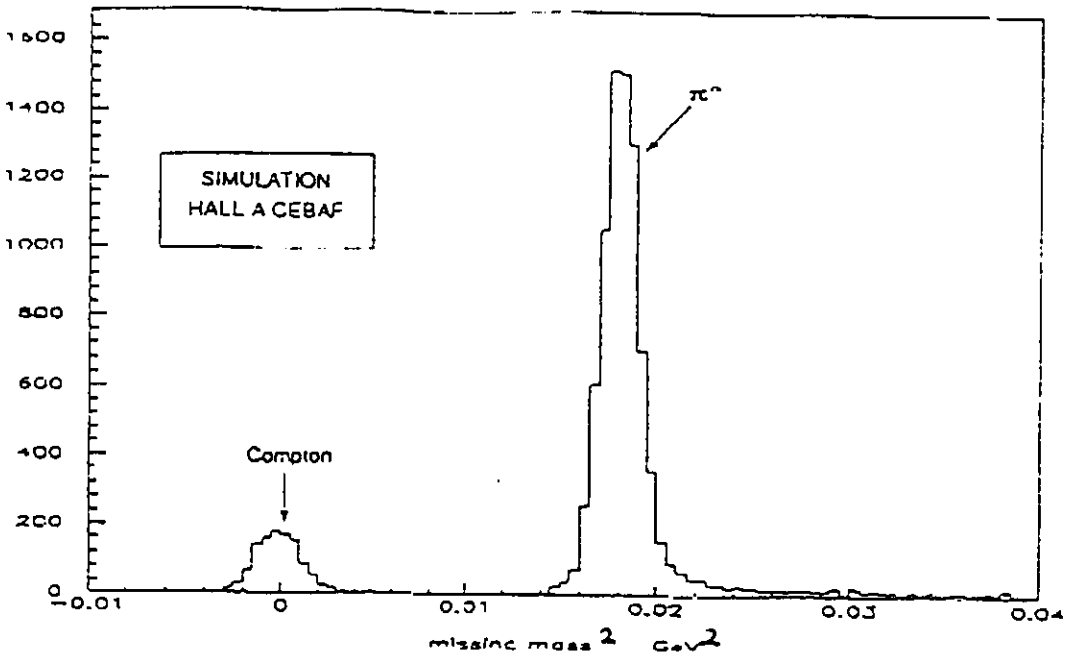

Figure 5: Missing mass squared spectrum for the reaction $p(e,e',p)X$.

3.2.1 VCS cross section evaluation from real photon data

The cross section of VCS, when the BH amplitude is negligible, can be written as [13] :

$$\frac{d^5\sigma}{dk'd\Omega'_e dtd\phi} = \Gamma(k,k',\theta'_e) \times \frac{d^2\sigma(s,Q^2,t)}{dtd\phi} \tag{16}$$

where Γ is the virtual photon flux factor and $d^2\sigma(s,Q^2,t)/dtd\phi$ the cross section $\gamma^* p \rightarrow \gamma p$ of photoproduction by a virtual photon. We have :

$$\Gamma(k,k',\theta'_e) = \frac{\alpha}{2\pi^2}\cdot\frac{k'}{k}\cdot\frac{(s-M^2)}{2M}\cdot\frac{1}{Q^2}\cdot\frac{1}{(1-\epsilon)} \tag{17}$$

$$\epsilon = (1+2\frac{\vec{q}^2}{Q^2}\tan^2\theta'/2)^{-1} \tag{18}$$

$$\frac{d^2\sigma(s,Q^2,t)}{dtd\phi} = \frac{d\sigma_T}{dtd\phi} + \epsilon\frac{d\sigma_L}{dtd\phi} + \epsilon\frac{d\sigma_{TT}}{dtd\phi}\cos 2\phi + \sqrt{\epsilon(1+\epsilon)}\frac{d\sigma_{LT}}{dtd\phi}\cos\phi \tag{19}$$

The cross sections were extrapolated from real Compton scattering data (Figure 2 and [2]) according to the following approximations :

1. Only the transverse part is taken into account:

$$d\sigma_L = 0,\ d\sigma_{TT} = 0,\ d\sigma_{LT} = 0$$

This strong assumption, which gives conservative counting rates, is supported by 2 facts :

- In the deep inelastic region, the ratio $R = \sigma_L/\sigma_T$ is small (≤ 0.2).
- In electroproduction of the pion the longitudinal part of the cross section is important only at low value of t ($|t| < .3GeV^2$) and the interference parts σ_{TT} and σ_{LT} are always small [13].

2. We neglect any dependence in $\cos\theta^{\gamma}_{cm}$ for the $\gamma^* p \rightarrow \gamma p$ cross section. The value of the cross section $d\sigma_T/dt$ is taken at $\theta^{\gamma}_{cm} = 90^0$, angle between the scattered and virtual photon, where experimentally the cross section of real Compton seems to be minimum (Figure 2).

3. The s dependence is taken as s^{-6} according to the scaling law which is approximately satisfied in our energy range by real Compton scattering (Figure 2).

4. No dependance on Q^2 is assumed for the $\gamma^* p \rightarrow \gamma p$ cross section which is taken equal to its value at $Q^2 = 0$. This is consistent with the Deep Inelastic Scattering $\gamma^* p \rightarrow X$ cross section at high energy.

In summary, we have taken :

$$2\pi s^6 \frac{d\sigma_T(Q^2, s, t)}{dt d\phi} = 30\mu b \cdot GeV^{10} \tag{20}$$

3.2.2 VCS cross section prediction from diquark model

The diquark model has been successfully used for calculating processes in the medium hard transfer region. Recently, measurements of $\gamma\gamma \rightarrow p\bar{p}$ cross section at CLEO were very well reproduced by calculations based on diquark model [11].

Compared to the extrapolation of real Compton data described previously, the diquark model has significantly different predictions for Q^2, s and t dependence of the VCS cross section. Figure 6 shows a comparison of the cross section dependence on $\cos\theta_{CM}$ at fixed $Q^2 = 1(GeV/c)^2$, $s = 5(GeV/c)^2$.

Figure 7 shows the relative contribution from transverse,longitudinal transverse-transverse and transverse-longitudinal terms for $Q^2 = 0.8(GeV/c)^2$, $s = 5(GeV/c)^2$. The transverse term is largely dominating the cross section in the region $-0.7 < \cos\theta_{CM} < 0.7$.

Figure 8 shows the ratio of the diquark model VCS to the Bethe-Heitler cross section as a function of $\cos\theta_{CM}$ at $s = 5(GeV/c)^2$ for different values of Q^2 reachable at CEBAF. At backward angles of the outgoing photon in the center of mass system,

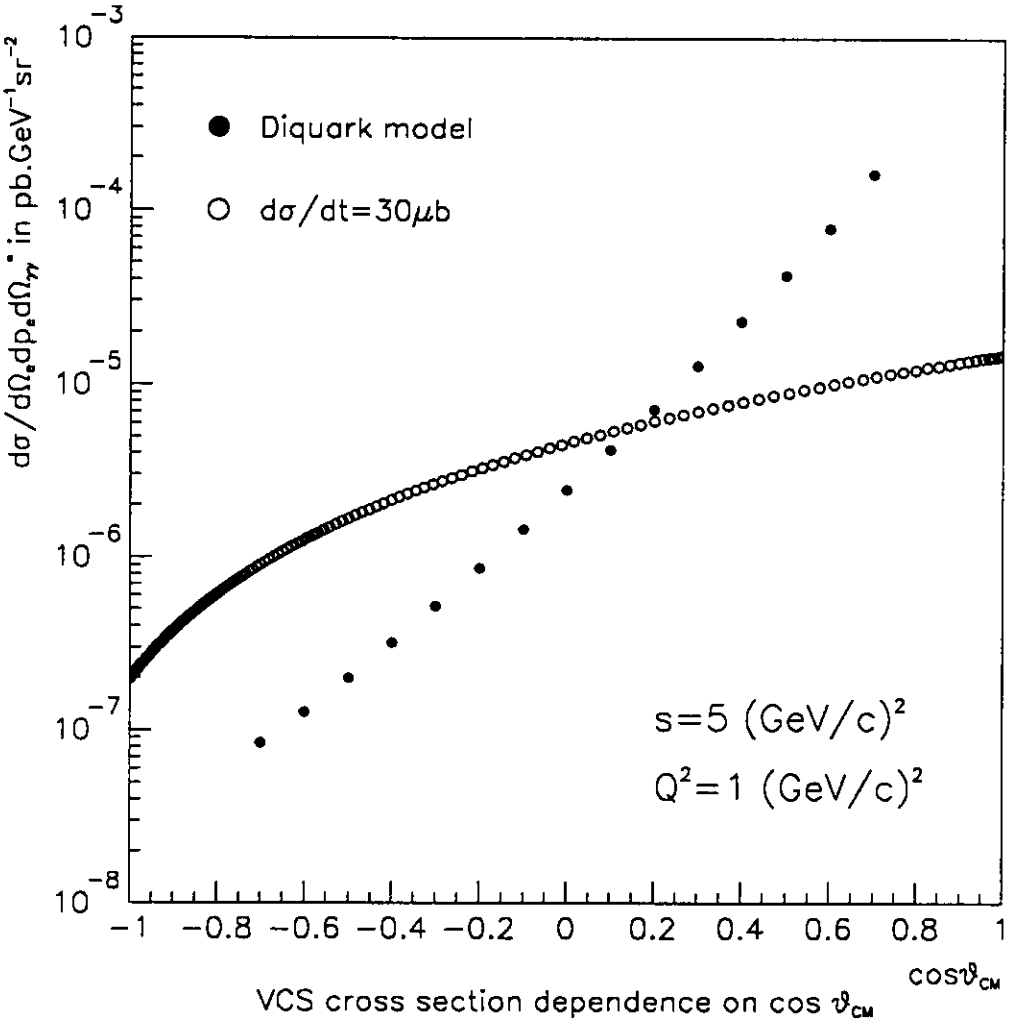

Figure 6: VCS cross section dependence on $\cos\theta_{CM}$ at fixed $Q^2 = 1(GeV/c)^2$, $s = 5(GeV/c)^2$ and $\phi = 0$: prediction from diquark model of [8] and extrapolation from real Compton data of [2].

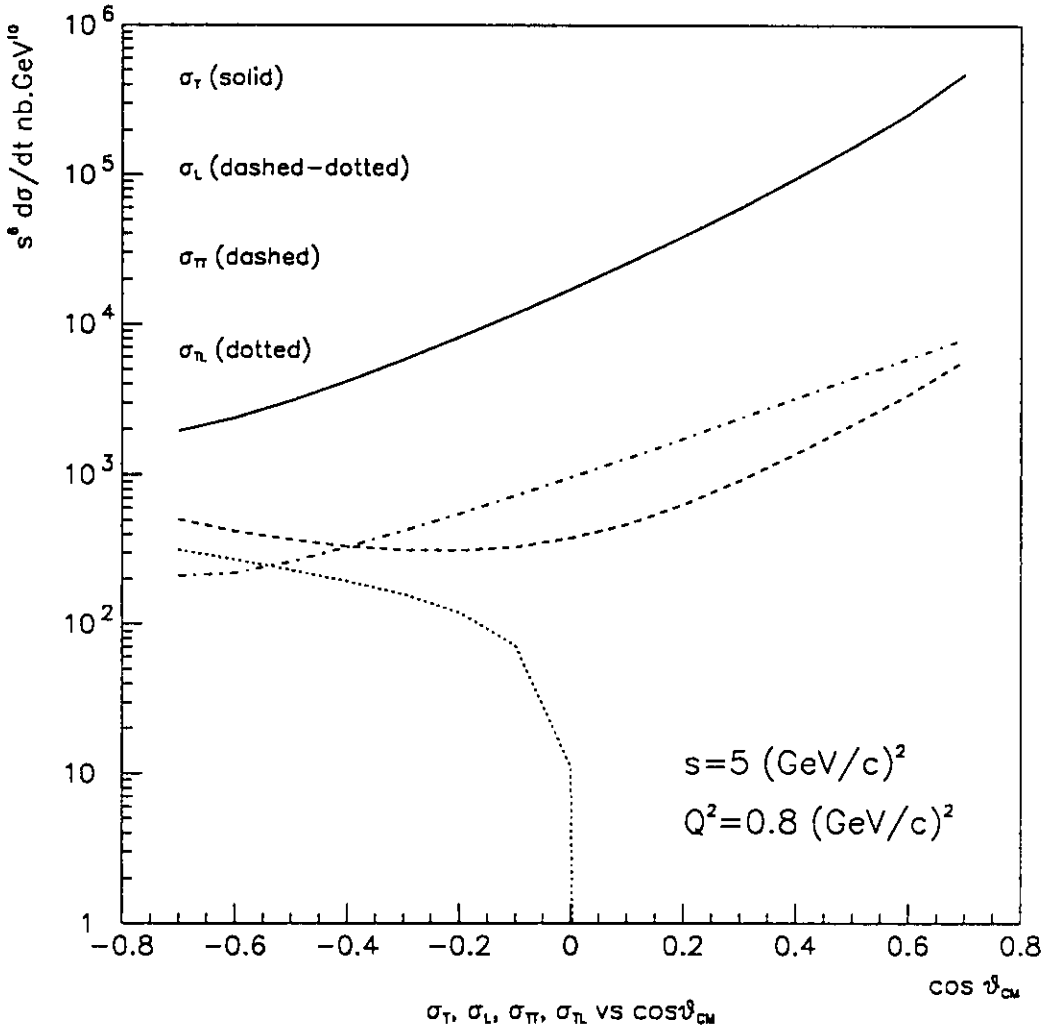

Figure 7: Contribution of transverse, longitudinal transverse-transverse and transverse-longitudinal terms to VCS cross section at $Q^2 = 0.8(GeV/c)^2$, $s = 5(GeV/c)^2$ $\phi = 0$, within diquark model.

the ratio is large so the VCS cross section can be extracted. The curve shows also the difficulty to extend measurements to forward angles as the ratio is much smaller than 1.

The diquark model has also definite predictions for the interference between VCS and Bethe-Heitler. Indeed, if we call A_{VCS} and A_{BH} the amplitudes of the VCS and BH processes for a given kinematics, the total cross section for $e + p \rightarrow e + p + \gamma$ is equal to

$$A_{VCS}^2 + A_{BH}^2 + 2\delta\sigma_{int} \tag{21}$$

where $\delta\sigma_{int}$ is the contribution from interference which is maximized when A_{VCS} and A_{BH} are comparable. In the kinematic region accessible at CEBAF, the interference is predicted to be dominantly destructive as can be seen from figure 9-a showing $\delta\sigma_{int}/|A_{VCS}||A_{BH}|$ for $s = 5(GeV/c)^2$ and different values of Q^2 for backward angle kinematics in the photon-proton center of mass.

Figure 9-b highlights another non-trivial behaviour of the interference within the diquark model. The interference varies very slowly with the beam energy at fixed Q^2, s and t (or θ_{CM}). This comes from the strong dominence of one $\gamma^* p \rightarrow \gamma p$ helicity amplitude.

The measurement of the interference and its dependence on beam energy at fixed Q^2, s and t (or θ_{CM}) would therefore be a crucial test of the diquark model, provided the interference term can be extracted from the cross section.

3.3 Proposed kinematics

We propose to study the dependence of VCS cross section on the photon momentum transfer Q^2 at fixed s and t (or θ_{CM}), on the transfer t at fixed Q^2 and s , and to select kinematics where to measure the interference between VCS and BH. The choice of the kinematics is based on a compromise between reaching the highest possible values of Q^2, s and p_t and keeping reasonnable counting rates.

For all the kinematics listed below, counting rates are given using the simple extrapolation from real Compton data described in 3.2.1 and the diquark model calculation from [8]. N_{comp} refers to the counting rate per hour using the extrapolation from real Compton data, as $N_{comp}^{diquark}$ refers to the counting rate using the diquark model. At backward angles, the 2 models disagree by about a factor 4 to 15. Beyond 135°, the diagrams taken into account by the diquark model are expected to become underdominent, as diffractive Compton production becomes important : we used the extrapolation from real Compton data to estimate counting rates for these kinematics.

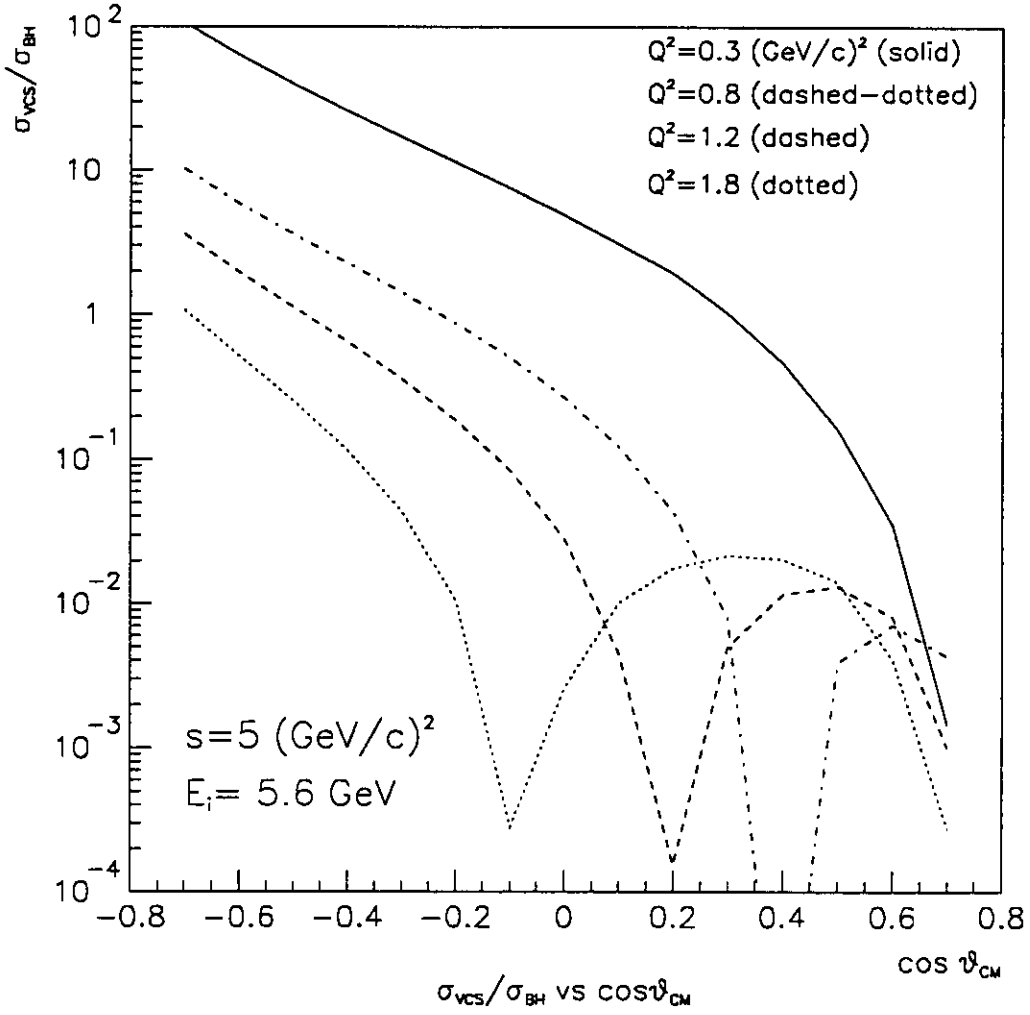

Figure 8: ratio of the VCS cross section calculated within diquark model to the Bethe-Heitler cross section as a function of $\cos\theta_{CM}$ at $s = 5(GeV/c)^2$, $\phi = 0$ for different values of Q^2 reachable at CEBAF. Beam incident energy is taken equal to 5.6 GeV.

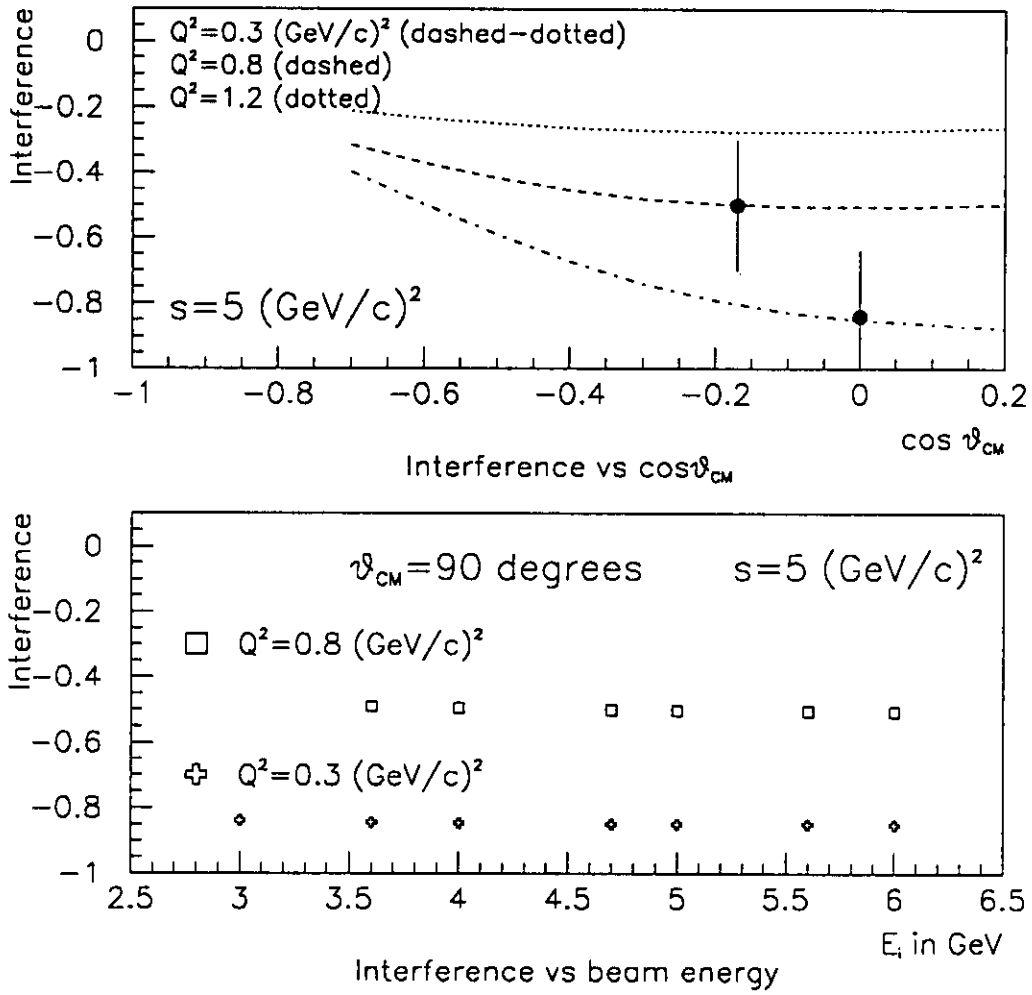

Figure 9: a- $\delta\sigma_{int}/|A_{VCS}||A_{BH}|$ as a function of $cos\theta_{CM}$ for $s = 5(GeV/c)^2$ and different values of Q^2 calculated within diquark model of [8] at $\phi = 0$. The two data points show the statistical errors from the measurements in this proposal.
b- Beam energy dependence of the interference at $s = 5(GeV/c)^2$, $\theta_{CM} = 90°$, $Q^2 = 0.8(GeV/c)^2$ and $Q^2 = 0.3(GeV/c)^2$, within diquark model.

3.3.1 Angular dependence at $s = 5\ (GeV/c^2)$ and $Q^2 = 0.3\ (GeV/c^2)$ and $Q^2 = 0.8\ (GeV/c^2)$

The purpose of these distributions is to compare the onset of perturbative QCD as a function of the transverse momentum at $Q^2 = 0.3\ (GeV/c^2)$ (see table 1) and $Q^2 = 0.8\ (GeV/c^2)$ (see table 2), to learn about the influence of the photon virtuality.

At forward angles, the distribution is extended up to the angle where the VCS cross section predicted by the diquark model is about 1/10 of the Bethe-Heitler cross section. We thereby insure we cover the region of strong VCS-BH interference.

At backward angles beyond 135°, focusing effects from the CM to lab boost increase the acceptance in the azimuthal angle ϕ and the counting rates.

E_i GeV	t (GeV/c^2)	θ_e °	θ_γ^{CM} °	θ_p °	P_t GeV/c	N_{comp} c/h	N_{beth} c/h	$N_{comp}^{diquark}$ c/h
3.95	-0.94	12.5	60	-55.24	0.80	22	5800	150.
3.95	-1.23	12.5	70	-50.33	0.86	37	725	100.
3.95	-1.55	12.5	80	-45.6	0.91	35	111	66.
3.95	-1.87	12.5	90	-41.17	0.92	42	34	51.
3.95	-2.19	12.5	100	-36.92	0.91	70	11	38.5
3.95	-2.51	12.5	110	-32.88	0.86	76	4	28.
3.95	-2.80	12.5	120	-29.03	0.80	80	2	25.
3.95	-3.07	12.5	130	-25.33	0.70	86	1.2	32.
3.95	-3.30	12.5	140	-21.76	0.60	104	0.5	-
3.95	-3.50	12.5	150	-18.29	0.46	98	0.36	-
3.95	-3.63	12.5	160	-14.89	0.31	104	0.28	-

Table 1: Angular dependence of VCS cross section at $s = 5\ (GeV/c^2)$ and $Q^2 = 0.3\ (GeV/c^2)$

3.3.2 Q^2 dependence

We propose to study the Q^2 dependence of the VCS cross section at $s = 5\ (GeV/c^2)$ and $\theta_{CM} = 110°$ corresponding to $P_t = 0.87\ (GeV/c)$ (see table 3). At fixed s and θ_{CM}, the transverse momentum is fixed and does not depend on Q^2. We will use the kinematics already measured at $Q^2 = 0.3\ (GeV/c^2)$ and $Q^2 = 0.8\ (GeV/c^2)$ for angular dependence and add a measurement at $Q^2 = 1.2\ (GeV/c)^2$.

E_i GeV	t (GeV/c^2)	θ_e $^\circ$	θ_γ^{CM} $^\circ$	θ_p $^\circ$	P_t GeV/c	N_{comp} c/h	N_{beth} c/h	$N_{comp}^{diquark}$ c/h
5.5	-1.8	12.9	80	-46.8	0.91	70	2368	102
5.5	-2.17	12.9	90	-42.9	0.92	103	230	61
5.5	-2.54	12.9	100	-39.13	0.91	132	53	42
5.5	-2.9	12.9	110	-35.53	0.87	152	20	38
5.5	-3.24	12.9	120	-32.1	0.8	180	7.2	26
5.5	-3.54	12.9	130	-28.8	0.70	200	2.9	23
5.5	-3.81	12.9	140	-25.6	0.59	234	1.5	-
5.5	-4.02	12.9	150	-22.4	0.46	246	1	-
5.5	-4.18	12.9	160	-19.4	0.31	246	.64	-
5.5	-4.27	12.9	170	-16.4	0.16	254	.4	-
5.5	-4.31	12.9	180	-13.4	0.0	242	0.34	-

Table 2: Angular dependence of VCS cross section at $s = 5\ (GeV/c^2)$ and $Q^2 = 0.8\ (GeV/c^2)$

E_i GeV	Q^2 (GeV/c^2)	t (GeV/c^2)	θ_e $^\circ$	θ_{CM} $^\circ$	θ_p $^\circ$	N_{comp} c/h	N_{beth} c/h	$N_{comp}^{diquark}$ c/h
3.95	0.3	-2.51	12.5	110	-32.88	76	4	28
5.5	0.8	-2.9	12.9	110	-35.53	152	20	38
6.	1.2	-3.2	14.4	110	-35.52	126	32	22

Table 3: Q^2 dependence of VCS cross section at $s = 5\ (GeV/c^2)$ and $\theta_\gamma^{CM} = 110^\circ$

3.3.3 Measurement of the interference between VCS and BH

The choice of the kinematics to measure the interference depends heavily on the validity of the cross sections derived from our models. Table 4 gives a list of kinematics where such a separation could be done in the hypothesis that the cross sections from diquark model are correct. If the theoretical cross sections are wrong, the study of θ_{CM} dependences presented before will give enough information to select other favourable kinematics.

For each set of values for Q^2, s and t, we propose 3 different kinematics at different beam energies giving therefore different σ_{VCS}/σ_{BH} ratios. We propose to extract the VCS cross section and the interference term from these measurements.

E_i GeV	Q^2 (GeV/c^2)	s (GeV/c^2)	t (GeV/c^2)	θ_γ^{CM} $^\circ$	P_t GeV/c	N_{beth} c/h	$N_{comp}^{diquark}$ c/h
3.95	0.3	5	-1.87	90	0.92	35	52
3.6	0.3	5	-1.87	90	0.92	25	22.5
3.	0.3	5	-1.87	90	0.92	24	5
5.5	0.8	5	-2.54	100	0.91	53	42
5.	0.8	5	-2.54	100	0.91	55	27
4.	0.8	5	-2.54	100	0.91	46	7
5.	0.8	4	-2.27	110	0.73	73	85
4.	0.8	4	-2.27	110	0.73	59	32
3.	0.8	4	-2.27	110	0.73	52	4

Table 4: Kinematics to extract the interference between VCS and BH

On figure 9-a are plotted very conservative estimates of the error bars one could get on the interference with 80 hours beam time for each of the 2 sets of 3 kinematics at $s = 5(GeV/c)^2$ in table 4.

3.4 Background from (e, e', π^0)

The width of the photon invariant mass peak $\sigma(M_X^2)$ was estimated taking into account multiple scattering and electron bremsstrahlung. Due to the excellent resolution of Hall A spectrometers, the ratio $m_{\pi^0}^2/\sigma(M_X^2)$ of the pion mass squared to the width of the photon peak ranges from 6 to 9 for all kinematics listed in the tables, allowing a clean separation between VCS and π^0 events.

3.5 Backgrounds

Accidental coincidences were estimated from single electron and proton counting rates using a Monte-Carlo simulation of Hall A spectrometers by Pierre Bertin [12]. Our single electron counting rate takes into account elastic cross section on the proton, electroproduction of Δ and two resonances at $\sqrt{s} = 1.5$ and 1.7 GeV. Our proton counting rate is dominated by photoproduction. Rates for accidental coincidences were estimated with the following assumptions :

- Electrons and protons are fully identified, and all the others are rejected.
- The peak of time coincidence between the two arms has a 2 nanoseconds full width.
- We require the two particles to originate from the same point within the target within $\pm 2\sigma$ resolution. The transverse resolution for each spectrometer is 1mm FWHM (table 4.1 of [10]) and we assume that the spectrometers see an effective target length of 100mm.

These timing and spatial requirements ensure a very low level of accidental coincidences.

4 Beam time request

The beam time request is presented on table 5. For each kinematics defined by the incident beam energy E_i, Q^2, s, t corresponding to a given θ_{CM}, P_t, a number of hours is given as well as the distance from the π^0 peak expressed in units of $m^2_{\pi^0}/\sigma(M_X^2)$. Some kinematics are used for several studies. The different parts in the table correspond to the programs :

- Part I: angular dependence at $Q^2 = 0.3(GeV/c)^2$, $s = 5(GeV/c)^2$.
- part II: angular dependence at $Q^2 = 0.8(GeV/c)^2$, $s = 5(GeV/c)^2$,
- part III: Q^2 dependence at $s = 5(GeV/c)^2$, $\theta_{CM} = 110°$
- part IV: interference between Bethe-Heitler and Virtual Compton scattering.

We request a total beam time of **600 hours**. Including contingency, this corresponds to 28 days beam in the hall A at a maximum energy of 6 GeV and 80 μA current.

5 Future developments

We realize this proposal is just the beginning of the investigation of Virtual Compton Scattering above the resonance region. To go further in Q^2 or s, we are limited by count rate and beam energy. The present experiment will provide an essential benchmark to determine the practical limits in Q^2 and s at CEBAF or other future facilities.

In addition, we would like to make a more complete coverage of the angular distribution at fixed Q^2 and s. However, in order to go to values of θ_{CM} smaller than 80°, we find ourselves in the situation of either a BH amplitude much larger than the VCS amplitude ($\phi = 0$) or the proton and electron spectrometers interfering with each other ($\phi = \pi$). This difficulty can be alleviated with the use of the symmetric small angle chicane proposed for Hall-A (see *e.g.* Proposal "High Resolution 1 p-shell Hyper-Nuclear Spectroscopy", this PAC). Indeed, for a given value of Q^2 and s, the ratio of the VCS amplitude to the Bethe-Heitler amplitude increases with the beam energy. The absolute value of VCS cross section is larger too because, at fixed Q^2 and s, the virtual photon flux increases with energy. But this means that a full use of beam energy capabilities requires the possibility to detect the electron scattered at low angle.

The small angle chicane would significantly improve the range of $(e, e'p)\gamma$ measurements accessible at CEBAF.

References

[1] S.J. Brodsky and G. R. Farrar, Phys Rev Lett **31** (1973) 1153.

[2] M.A. Shupe et al., Phys Rev **D19** (1979) 1929.

[3] G.R. Farrar and E. Maina, Phys Lett **B206** (1988) 120.

[4] A.S. Kronfeld and B. Nižić, Phys Rev **D44** (1991) 3445.

[5] Glennys R. Farrar and Huayi Zhang, Phys Rev Lett **65** (1990) 1721. Glennys R. Farrar and Huayi Zhang, Phys Rev **D41** (1990) 3348.

[6] A. Pang and C.-R. Ji, BAPS **39** (1994) 1421

[7] P. Kroll, W. Schweiger and M. Schürmann, Z. Phys. **A338** (1991) 339.

[8] P. Kroll, M. Schürmann and P. Guichon, to be published

[9] P. Kroll, Th. Pilsner, M. Schürmann and W. Schweiger, Phys. Lett. **B316** (1993) 546.

[10] Conceptual Design Report, CEBAF, April 1990

[11] M. Artuso et al, CLEO collaboration, Phys. Rev. **D50** (1994) 5484.

[12] P.Y. Bertin, private communication, LPC Clermont-Ferrand, France

[13] P. Brauel et al, Z. Phys. **C3** (1979) 101.

[14] C. Coriano, A. Radyushkin, and G. Sterman, Nucl Phys **B405** (1993) 481; and C. Coriano, H. Li, Phys Lett **B324** (1994) 98.

[15] I. Musatov, A. Afanasev, and A. Radyushkin, private communication 1994.

[16] Nucleon structure study by Virtual Compton Scattering, proposal PR-93-050 to CEBAF PAC7, December 1993

E_i GeV	Q^2 (GeV/c^2)	s (GeV/c^2)	t (GeV/c^2)	θ_{CM} °	P_t GeV/c	$m^2_{\pi^0}/\sigma(M^2_X)$	Time hours
I							
3.95	0.3	5	-0.94	60	0.80	5	10
3.95	0.3	5	-1.23	70	0.86	5.3	10
3.95	0.3	5	-1.55	80	0.91	5.5	10
3.95	0.3	5	-1.87	90	0.92	5.7	15
3.95	0.3	5	-2.19	100	0.91	5.8	15
3.95	0.3	5	-2.51	110	0.86	5.9	15
3.95	0.3	5	-2.80	120	0.80	6.2	15
3.95	0.3	5	-3.07	130	0.70	6.7	20
3.95	0.3	5	-3.30	140	0.60	7.6	20
3.95	0.3	5	-3.50	150	0.46	8.9	15
3.95	0.3	5	-3.63	160	0.31	11.6	15
II							
5.5	0.8	5	-1.8	80	0.91	5.9	10
5.5	0.8	5	-2.17	90	0.92	6.1	15
5.5	0.8	5	-2.53	100	0.91	6.2	15
5.5	0.8	5	-2.9	110	0.87	6.4	20
5.5	0.8	5	-3.24	120	0.8	6.6	20
5.5	0.8	5	-3.54	130	0.7	7.1	20
5.5	0.8	5	-3.81	140	0.6	7.8	20
5.5	0.8	5	-4.02	150	0.46	9.2	20
5.5	0.8	5	-4.18	160	0.31	11.6	20
5.5	0.8	5	-4.27	170	0.16	17.3	20
5.5	0.8	5	-4.31	180	0.	34.6	20
III							
3.95	0.3	5	-2.51	110	0.86	5.9	-
5.5	0.8	5	-2.9	110	0.87	6.4	-
6.	1.2	5	-3.2	110	0.87	6.8	20
IV							
3.95	0.3	5	-1.87	90	0.92	5.6	-
3.6	0.3	5	-1.87	90	0.92	5.8	30
3.	0.3	5	-1.87	90	0.92	6.05	30
5.5	0.8	5	-2.54	100	0.91	6.2	20
5.	0.8	5	-2.54	100	0.91	6.4	30
4.	0.8	5	-2.54	100	0.91	6.6	30
5.	0.8	4	-2.27	110	0.73	8.11	20
4.	0.8	4	-2.27	110	0.73	8.7	30
3.	0.8	4	-2.27	110	0.73	8.9	30

Table 5: Beam time request

BEAM REQUIREMENTS LIST

CEBAF Proposal No.: _____ Date: 12/15/94

(For CEBAF User Liaison Office use only.)

List all combinations of anticipated targets and beam conditions required to execute the experiment. (This list will form the primary basis for the Radiation Safety Assesment Document (RSAD) calculations that must be performed for each experiment.)

Condition #	Beam Energy ~~(MeV)~~ GeV	Beam Current (μA)	Polarization and Other Special Requirements (e.g., time structure)	Target Material (use multiple rows for complex targets — e.g., w/windows)	Target Material Thickness (mg/cm²)
1	3.0	80μA	≥ 90% duty	Hall A	(10cm)
2	3.6	↓		High power	0.8 g/cm²
3	4.0			LH_2 target	
4	5.0				
5	5.5				
6	6.0	↓		↓	↓

e beam energies, E_{Beam}, available are: $E_{Beam} = N \times E_{Linac}$ where N = 1, 2, 3, 4, or 5. For 1995, E_{Linac} = 800 MeV, i.e., available E_{Beam} ar), 1600, 2400, 3200, and 4000 MeV. Starting in 1996, in an evolutionary way (and not necessarily in the order given) the following ditional values of E_{Linac} will become available: E_{Linac} = 400, 500, 600, 700, 900, 1000, 1100, and 1200 MeV. The sequence and ning of the available resultant energies, E_{Beam}, will be determined by physics priorities and technical capabilities.

Proposal No.: _____ Date: 12/15/94
(For CEBAF User Liaison Office use only)

.ck all items for which there is an anticipated need.

Cryogenics
- _____ beamline magnets
- _____ analysis magnets
- ✓ target
  - type: LH_2
  - flow rate: _____
  - capacity: _____

Hall A target

Electrical Equipment
- _____ cryo/electrical devices
- _____ capacitor banks
- _____ high voltage
- _____ exposed equipment

Radioactive/Hazardous Materials
List any radioactive or hazadorous/ toxic materials planned for use:
_____
_____
_____
_____

Pressure Vessels
- _____ inside diameter
- _____ operating pressure
- _____ window material
- _____ window thickness

Flammable Gas or Liquids
- type: _____
- flow rate: _____
- capacity: _____

Drift Chambers
- type: _____
- flow rate: _____
- capacity: _____

Other Target Materials
- ___ Beryllium (Be)
- ___ Lithium (Li)
- ___ Mercury (Hg)
- ___ Lead (Pb)
- ___ Tungsten (W)
- ___ Uranium (U)
- ___ Other (list below)

_____
_____

Vacuum Vessels
- _____ inside diameter
- _____ operating pressure
- _____ window material
- _____ window thickness

Radioactive Sources
- _____ permanent installation
- _____ temporary use
- type: _____
- strength: _____

Large Mech. Structure/System
- _____ lifting devices
- _____ motion controllers
- _____ scaffolding or
- _____ elevated platforms

Lasers
- type: _____
- wattage: _____
- class: _____

Installation:
- _____ permanent
- _____ temporary

Use:
- _____ calibration
- _____ alignment

Hazardous Materials
- ____ cyanide plating materials
- ____ scintillation oil (from)
- ____ PCBs
- ____ methane
- ____ TMAE
- ____ TEA
- ____ photographic developers
- ____ other (list below)

_____
_____

General:

Experiment Class:
- _____ Base Equipment
- _____ Temp. Mod. to Base Equip.
- _____ Permanent Mod. to Base Equipment
- _____ Major New Apparatus

Other: _____
_____

Us

LAB RESOURCES REQUIREMENTS LIST

CEBAF Proposal No.: _____ Date: _____
(For CEBAF User Liaison Office use only.)

List below significant resources — both equipment and human — that you are requesting *from CEBAF* in support of mounting and executing the proposed experiment. Do not include items that will be routinely supplied to all running experiments, such as the base equipment for the hall and technical support for routine operation, installation, and maintenance.

Major Installations *(either your equip. or new equip. requested from CEBAF)*

_____

_____

_____

_____

_____

_____

_____

_____

_____

New Support Structures: _____

_____

_____

Data Acquisition/Reduction

Computing Resources: _____

_____

_____

New Software: _____

_____

_____

Major Equipment

Magnets _____

_____

Power Supplies _____

_____

Targets _____

_____

Detectors _____

_____

Electronics _____

_____

Computer Hardware _____

_____

Other _____

_____

Other

Standard Hall-A
high resolution 2-arm
configuration +
high power LH_2 target